



APR Turbulence and Diffusion Note No. 280

**The Transport of Water across the Tropopause  
by Convection: Cloud Resolving Studies**

by

**S.J. Woolnough**

**30<sup>th</sup> November 2001**

© Crown Copyright 2001

Met Office  
London Road  
Bracknell  
Berkshire, RG12 2SZ

This paper has not been published. Permission to quote from it should be obtained from the Head of Atmospheric Processes Research, Met Office.

# The Transport of Water across the Tropopause by Convection: Cloud Resolving Studies

Steven J. Woolnough

November 30, 2001

## Abstract

The transport of water across the tropopause by convection is investigated in the Met Office Cloud Resolving Model. The dominant convective source of stratospheric water vapour is found to be through the sublimation of ice transported across the tropopause in penetrating convective plumes. However this ice sublimation makes only a small contribution to the ice budget above the tropopause and as such its magnitude is likely to be very sensitive to the specification of the ice microphysics within the model.

## 1 Introduction

The correct representation of stratospheric humidity in numerical models is important in both Numerical Weather Prediction and Climate Modelling. In climate modelling the stratospheric water vapour can have a large radiative impact and its correct representation in both current climate and climate change simulations is important to correctly simulate not only the current radiation balance, but also the correct sensitivity to e.g. greenhouse gas forcing. Additionally the humidity can have a large impact on the rates of some chemical reactions and so a correct representation of the humidity is required for successful chemical modelling whether coupled or off-line. In NWP the initial conditions for a forecast run are based on a combination of observations and a first guess field, which is usually a short forecast valid at the analysis time. Observations of water vapour above the tropopause are scarce and initial water vapour fields at these levels are almost entirely first guess fields. If the forecast model used to generate the first guess has a poor representation of the stratospheric humidity then these errors will continue through into the analysis and then into the next forecast.

The mechanisms by which water vapour is transported across the tropopause are not well understood. The simplest model of water vapour transport across the tropopause is through the mean vertical circulation (Brewer 1949; Dobson 1956) with upward motion across the tropical tropopause and descent across the extra-tropical tropopause. In such a model the stratospheric water vapour mixing ratios will be limited by the saturation values at the tropopause (which in turn are determined by the tropopause temperature). Observations of the stratospheric water vapour are broadly consistent with this model, with the annual cycle and horizontal variations in tropical lower stratospheric water vapour broadly consistent with annual variations (e.g. Mote et al. 1995,1996) and horizontal variations (e.g. Jackson et al. 1998) of tropopause temperatures.

Whilst this model can explain the basic temporal and horizontal structure of stratospheric water vapour there is still much uncertainty in the detailed budget of stratospheric water vapour. In particular whether there are preferred locations for the cross tropopause transport in the tropics, and the role of isentropic transport from the tropical upper troposphere to the extratropical stratosphere. In addition to these considerations, the role that convection plays in the stratospheric water vapour budget is unclear. Kley et al. (1982) suggested that convective clouds which penetrate the tropopause can hydrate the stratosphere by the sublimation of ice. However, Danielsen (1982) proposed a mechanism for stratospheric dehydration by convective overshoots in which radiative heating at the base of ice anvils together with cooling at the top of the anvils leads to convective overturning in the clouds giving rise to deposition of ice in the clouds. The fall velocity of the ice crystals is increased leading to enhanced sedimentation and dehydration of the lower stratosphere.

The role that convection may play in stratospheric water vapour transport is investigated here in Cloud Resolving Modelling experiments. No radiative effects are included here and so Danielsen’s hypothesis, which involves mixing due to differential heating by radiation to produce the dehydrating effect of convection cannot be tested within the framework of these experiments. Section 2 describes the experimental design, the results of these experiments are presented in section 3 and some conclusions and suggestions for future modelling studies are presented in section 4.

## 2 Experimental Design

A series of experiments have been performed in the Met Office Cloud Resolving Model (CRM) to investigate the transport of water substance across the tropopause by convection. The CRM is an extension of the Large-Eddy Simulation Model (Derbyshire et al. (1994) and Brown et al. (1997)) to incorporate a representation of ice microphysics (documentation for the microphysics can be found within the documentation for Version 2.3 of the model (Gray et al. (2001)))

In these integrations the CRM is forced by an imposed cooling of  $4\text{K day}^{-1}$  below a specified inversion height. This cooling acts to destabilize the atmosphere to convection. Above the specified inversion height there is no temperature forcing. The temperature profile is initialized in such a way that the temperature and height of the inversion in the initial profile is approximately maintained through out the integration and there is no jump in temperature at the inversion. To achieve this requires some fine tuning of the specified temperature at the inversion to prevent the convection becoming too deep and significantly modifying the height at which the inversion occurs, if the specified inversion temperature is too low, or generating a discontinuity in temperature at the inversion, which would occur if the specified temperature is too warm. The required inversion temperature ends up being close to the temperature of a saturated moist adiabat raised from the surface to the level of the inversion.

Above the specified inversion height the moisture profile is relaxed towards a specified ‘dry’ profile (with a mixing ratio of  $1 \times 10^{-5} \text{g kg}^{-1}$ ) on a fixed timescale. Such a relaxation is designed to mimic the processes which act above the inversion to remove moisture from the inversion region. This choice of moisture forcing allows the model to come to an equilibrium in which the rate of removal of moisture comes into balance with the flux of water across the inversion from below. If a drying rate was specified then at equilibrium the rate of transfer across the inversion would have to balance the specified drying rate and any dependence of the rate on the properties of the inversion would be removed, instead the convection would

have to adjust the profile until it could balance the specified loss, or in some circumstances it would not be able to achieve this and no equilibrium would be reached. Below the inversion height there is no moisture forcing.

The model is run with a 2D domain of 256km in the horizontal direction, with a 1km resolution and 20km (with 60 gridpoints  $\sim 300\text{m}$  resolution in most of the domain) or 25km (75 gridpoints) in the vertical direction, depending on the height of the inversion, there is a 5km damping layer at the top of the model.

The surface fluxes are enhanced by specifying a horizontal wind of  $5\text{ms}^{-1}$  in the direction perpendicular to the model domain. This enhancement of the surface fluxes enables the model to move to equilibrium rapidly and provides a source of water to balance the precipitation without resulting in an unrealistically dry boundary layer.

Experiments with 3 inversion heights were performed for various surface temperatures. The different surface temperatures mean that for a fixed inversion height the inversion temperature is changed.

Experiments were performed with inversions at 10km, 13km and 15km and for sea surface temperatures (SST) of  $27^\circ\text{C}$  and  $29^\circ\text{C}$  and additionally at  $25^\circ\text{C}$  for the 10km inversion experiment. The experiments are labelled ZZKSSC where ZZ is the inversion height and SS is the surface temperature.

## 3 Results

### 3.1 Equilibrium Profiles

Figure 1 shows the temperature profiles for each of the experiments. Although the details of the temperature profile around the specified inversion level are slightly different in each of the integrations the basic structure is the same and there is a strong inversion at the specified level. Figure 2 shows the total water profiles for each of the integrations, the upper panel shows a magnification of the region around the inversion in each case. For a given height of the inversion the water vapour mixing ratios above the inversion level decrease as the temperature decreases. In addition to this, as the inversion height increases the water vapour mixing ratios above the inversion decreases. However as the inversion height increases the temperature at the inversion decreases, so the dependence of the water vapour mixing ratio on both inversion height and temperature could simply be a reflection of the temperature effect on the saturation mixing ratio.

### 3.2 The water vapour budget above the inversion

The vertically integrated water vapour budget can be written as

$$\begin{aligned} \frac{\partial}{\partial t} \left( \int_{z_1}^{z_2} \rho_s q_n dz \right) &= \rho_s(z_1) [\overline{wq_n^r}(z_1) + \overline{wq_n^{sg}}(z_1)] - \rho_s(z_2) [\overline{wq_n^r}(z_2) + \overline{wq_n^{sg}}(z_2)] \\ &\quad + \int_{z_1}^{z_2} \rho_s (Q_{force} + Q_{micro}) dz + f_n(z_1) - f_n(z_2) \end{aligned} \quad (1)$$

where  $q_n$  is a particular water species mixing ratio,  $\overline{wq^r}$  and  $\overline{wq^{sg}}$  are the resolved and sub-grid vertical fluxes of the species,  $Q_{force}$  and  $Q_{micro}$  are the tendencies of the species due to the large-scale forcing and microphysics and  $f_n$  is the flux due to sedimentation (positive upwards for consistency). The large-scale forcing term is only non-zero in the budget for the total water variable (vapour + cloud liquid),  $q_t$ , and the sedimentation term is zero in the budget for this variable.

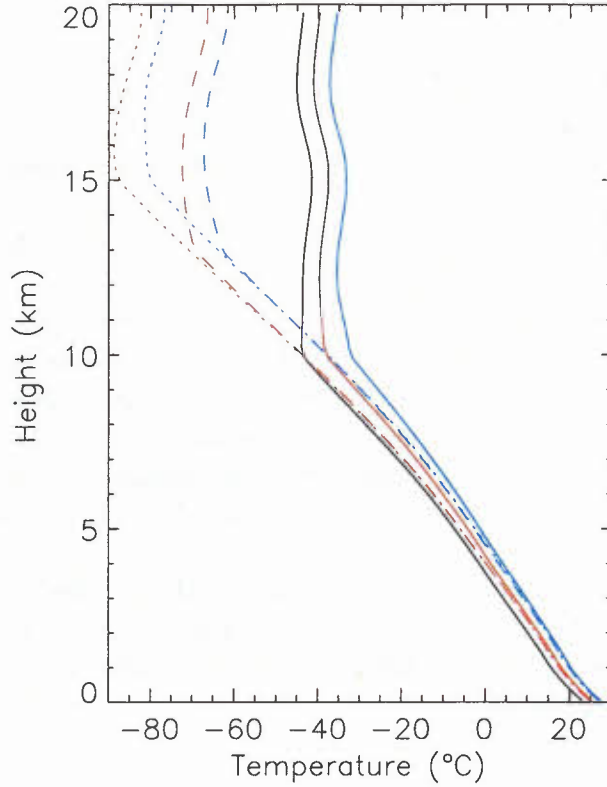


Figure 1: Temperature profiles for each of the integrations with SSTs of 25°C (black line), 27°C (red lines) and 29°C (blue lines) with inversion heights of 10km (solid lines), 13km (dashed lines) and 15km (dotted lines).

TERM ( $\text{g m}^{-2} \text{ day}^{-1}$ )	10K29C	10K27C	10K25C	13K29C	13K27C	15K29C	15K27C
Resolved Flux	+185.6	+89.52	+23.51	+2.68	+0.824	+0.268	+0.1172
Sub-grid Flux	+4.6	+1.50	+0.87	+0.36	+0.163	+0.024	+0.0144
Microphysics	-46.2	+4.61	+28.92	+10.35	+5.608	+0.911	+0.3531
Forcing	-141.3	-91.68	-55.10	-12.43	-6.316	-1.173	-0.4746
Tendency	+4.5	+2.39	-1.49	+1.07	+0.322	+0.044	+0.0150
Error	-1.8	+1.56	-0.31	-0.11	-0.043	-0.015	-0.0049

Table 1: Terms in the vertically integrated budget of the total water variable,  $q_t$ , (vapour + cloud liquid) above the level of the imposed inversion. The error term is the difference between the observed tendency and the sum of the diagnosed terms in the budget. The units are  $\text{g m}^{-2} \text{ day}^{-1}$ . The columns are ordered such that the temperature at the inversion decreases from left to right.

Table 1 shows the budget for the total water variable above the level of the imposed inversion in each of the integrations, the fluxes out of the top of the domain are zero. The dominant terms in the budget are the forcing, the resolved flux and the microphysics. For the integrations in which the inversion is at 10km there is a significant difference in the balance of the budget depending on the temperature of the inversion. In the warmest integration, with an SST of 29°C there is a net removal of water vapour and cloud liquid by the microphysics and the resolved flux vapour and liquid across the inversion more than balances the forcing.  $37\text{g m}^{-2} \text{ day}^{-1}$  of the water transported across the inversion in this integration is as cloud liquid. In the integration with an SST of 27°C the resolved flux of water vapour and cloud liquid across the inversion almost exactly balances the large-scale forcing, although there is a small source of  $q_t$  due to the microphysics.  $17\text{g m}^{-2} \text{ day}^{-1}$  of the resolved flux across the



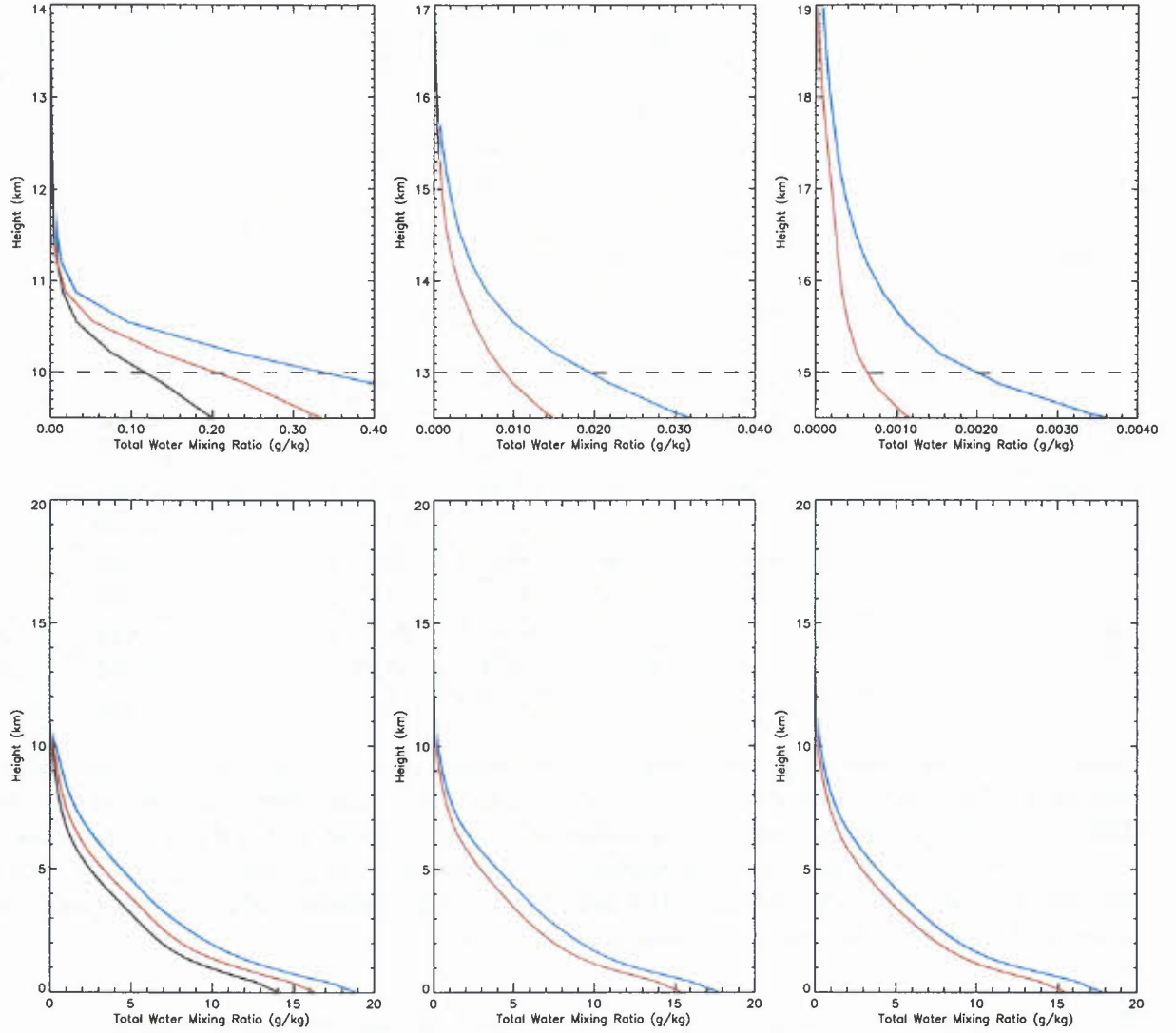


Figure 2: The equilibrium total water mixing ratio  $q_t$ , in each integration. From left to right, the panels are for the integrations with an inversion at 10km, 13km and 15km respectively. The blue lines are the integrations with an SST of 29°C, the red lines are the integrations with an SST of 27°C and the black line in the lefthand column is for the integration with an SST of 25°C. The upper panels show a magnification around the region of the inversion, indicated by the dashed line.

inversion is cloud liquid. For the integration with an SST of 25°C the microphysical source of  $q_t$  and the flux of  $q_t$  across the inversion are comparable and between them balance the drying by the large-scale forcing. There is no flux of cloud liquid water across the inversion in this experiment.

The temperatures at the inversion in these three integrations are -29°C, -35°C and -41°C respectively. The micro-physical scheme in the CRM assumes that there is instantaneous homogeneous freezing of cloud-liquid at temperatures below -38°C. The 10K25C integration and all the other integrations with higher inversions have inversion temperatures below this threshold and as such there is no transport of cloud liquid across the inversion and no cloud liquid above the inversion. The two integrations where cloud liquid is present at the inversion will be referred to as the ‘warm integrations’ and the remaining five will be referred to as the ‘cold integrations’.

Because of the difference in the nature of the microphysics between the warm and cold integrations and because the tropopause in regions where the SST is as high as 27°C or

TERM ( $\text{g m}^{-2} \text{ day}^{-1}$ )	10K29C	10K27C	10K25C	13K29C	13K27C	15K29C	15K27C
Resolved Flux	+14.58	+63.33	+89.41	+272.7	+267.9	+120.8	+176.3
Sub-grid Flux	-0.30	-0.53	+0.45	+3.0	+2.1	+1.7	+3.1
Microphysics	+11.24	-7.87	-29.48	-10.9	-5.8	-1.0	-0.4
Sedimentation	-23.85	-57.65	-59.23	-264.0	-257.8	-121.4	-180.5
Tendency	+0.00	-0.24	+1.39	+1.0	+5.4	+0.0	-2.3
Residual	+1.67	-2.48	-0.24	-0.2	+1.0	+0.1	+0.8

Table 2: As for Table 1 but for the vertically integrated budget of ice,  $q_i$ .

TERM ( $\text{g m}^{-2} \text{ day}^{-1}$ )	10K29C	10K27C	10K25C	13K29C	13K27C	15K29C	15K27C
IACW	+1.26	+0.30	+0.00	+0.00	+0.00	+0.000	+0.000
IDEP	+45.43	+48.06	+16.04	+16.06	+7.95	+1.701	+0.941
IPRM	+0.00	+0.00	+0.00	+0.00	+0.00	+0.001	+0.004
IFRW	+2.64	+1.93	+0.00	+0.00	+0.00	+0.000	+0.000
SACI	-0.84	-0.99	-0.66	-0.48	-0.22	-0.043	-0.028
GACI	-0.04	-0.05	-0.03	-0.02	-0.01	-0.002	-0.001
ISUB	-28.29	-56.29	-44.83	-26.42	-13.56	-2.613	-1.298
SAUT	-8.92	-0.84	-0.01	-0.02	-0.01	-0.004	-0.002
TOTAL	+11.24	-7.86	-29.48	-10.88	-5.85	-0.960	-0.384

Table 3: Non-zero terms in the vertically integrated budget of the ice microphysics terms above the inversion. For a full description of the terms and their functional form see Gray et al. (2001). IDEP and ISUB are the deposition and sublimation of ice. IPRM and IFRW are the conversion of cloud water to ice by heterogeneous nucleation and homogeneous freezing respectively. IACW is the collection of cloud water by ice. SACI and GACI are the collection of ice by snow and graupel respectively. SAUT is the autoconversion of ice to snow.

29°C is observed to be much higher than 10km the following analysis will focus on the cold integrations. Some results from the warm experiments will be included for completeness.

In the experiments with inversions at 13km and 15km the dominant source of water vapour above the inversion is from the microphysics, with a smaller contribution from the transport of water vapour across the inversion. Analysis of the budgets for the hydrometeors reveals that the sublimation of ice is the main microphysical source of water vapour.

Table 2 shows the budget of the ice variable above the inversion. In the 10K25C experiment the microphysics term removes over 30% of the ice transported across the inversion, with the rest of the transport being balance by the sedimentation of ice across the inversion. In the integrations with higher inversions at 13km and 15km, almost all of the transport of ice across the inversion is balanced by the sedimentation term with a very small sink of ice from the microphysics. Table 3 shows the non-zero terms in the ice microphysics budget above the inversion The dominant terms in the ice microphysics budget for the cold integrations are the sublimation and deposition terms, but in each these experiments these two terms are of comparable magnitude and the net microphysical tendency is smaller in magnitude than either of these terms (except the 10K25C experiment).

These budgets show that the dominant source of water vapour above the inversion in the cold experiments, which are the most like tropical conditions, is the sublimation of ice. This sublimation of ice however is only a small term in the budget of the ice above the inversion, with most of the ice which is transport across the inversion simply sedimenting out. The net sublimation of ice is also a residual of larger sublimation and deposition terms within the microphysics budget. The water-vapour budget (and hence equilibrium water vapour

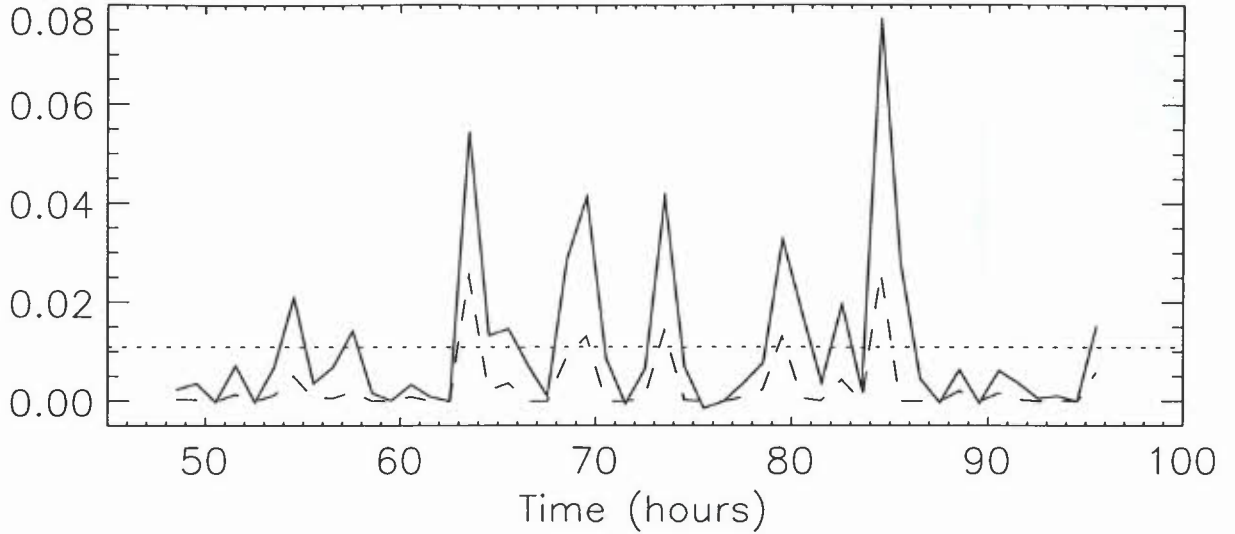


Figure 3: *Timeseries of the hourly averaged ice flux ( $\text{g kg}^{-1} \text{ m s}^{-1}$ ) at the level of the inversion (solid line) from the 13K27C integration. Graupel mixing ratio ( $\text{g kg}^{-1}$ ) at the level immediately below the inversion (dashed line). The dotted line shows the time mean ice flux across the inversion.*

content) above the inversion is therefore likely to be very sensitive to the details of both the representation of the ice microphysics within the model, as well as the specification of the ice fall speed.

Having shown that the dominant source of water vapour above the inversion to balance the large-scale forcing in these experiments is the sublimation of ice, the question remains as to how the ice is transported across the inversion? Is it through transports associated with the mixing of gravity waves or turbulence within the anvils associated with the convection or is it through penetration of strong convective plumes?

Figure 3 shows a timeseries of the flux of ice across the inversion for the experiment 13K27C. There is a high degree of temporal variability in the flux, with the time mean flux being made up of a number of periods with a large flux across the inversion and a number of periods with little or no transfer of ice across the inversion. The dashed line on the plot shows the times series of graupel mixing ratio at the level immediately below the inversion. These two timeseries are clearly correlated (the correlation coefficient is 0.94). The presence of graupel at this level (12.9km) is a good indication that there is strong and deep convection and the strong correlation between the graupel timeseries and the flux of ice across the inversion suggests that the transport of ice across the inversion is associated with deep convection.

Figures 4-7 show instantaneous cross-sections of the vertical velocity, ice mixing ratio and ice fluxes at different times from the same integration. In the top panel of figure 4 there is a single strong updraft, characteristic of newly developed deep convection. There is significant penetration of this plume above the level of the inversion and the plume becomes neutrally buoyant at the level of the inversion. The side panel shows the buoyant ( $\theta'_v > 0$ ) moist ( $q_v + q_l + q_i > q_{sat}$ ) updraft ( $w > 0$ ) mass flux, which becomes zero close to the level of the inversion.

The middle panel in figure 4 shows the ice mixing ratio cross section, there is a large amount of ice within in the plume with mixing ratios in excess of  $1 \text{ g kg}^{-1}$ . The bottom panel in figure 4 shows the vertical transport of ice, with a large transport of ice upwards across the inversion within the updraft and a small return transport in the downdrafts of the overturning circulation. The side panel shows the net vertical transport of ice at this time



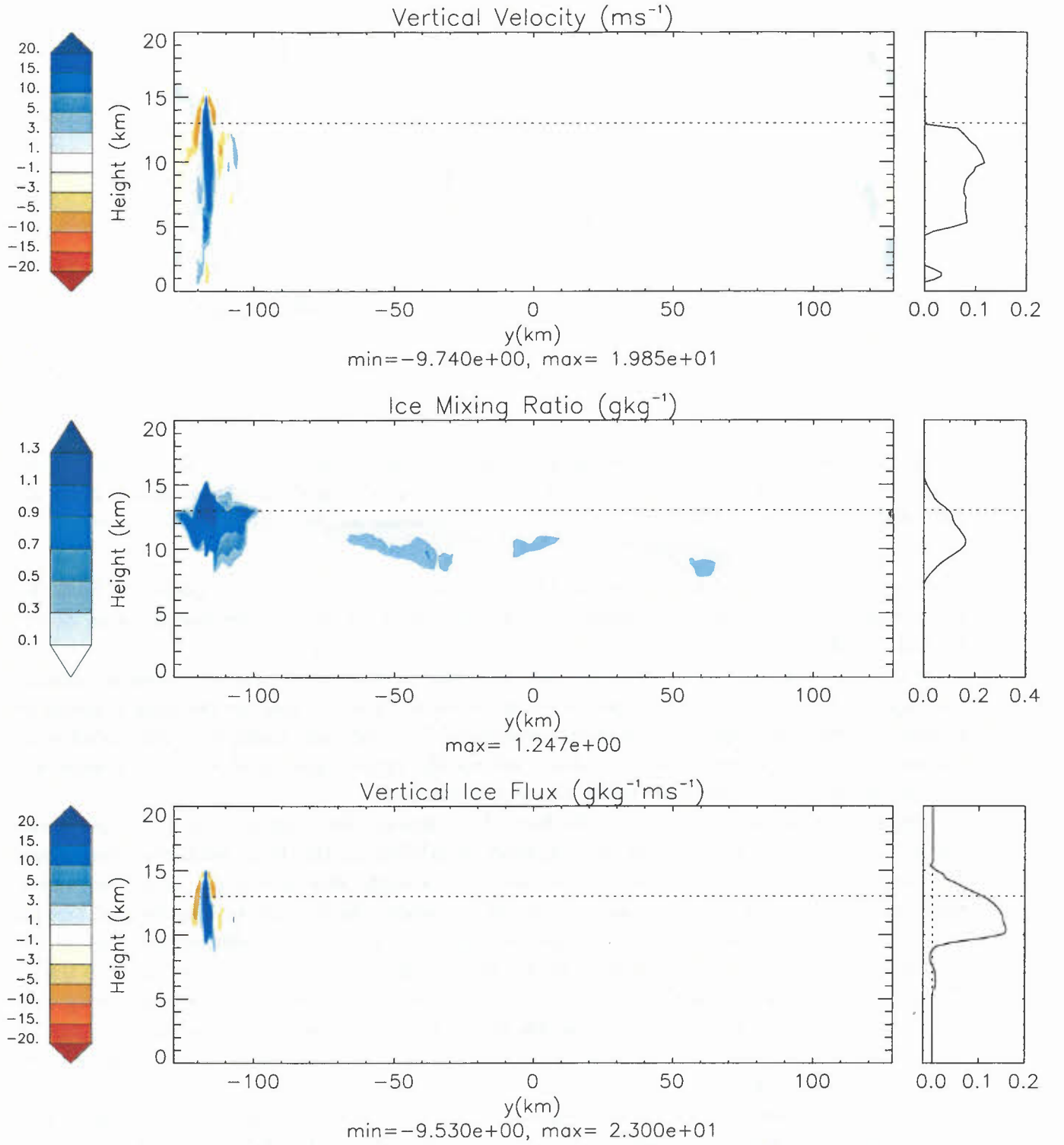


Figure 4: *Instantaneous fields from the 13K27C integration after 69 hours. The top panel shows the vertical velocity ( $\text{m s}^{-1}$ ). The middle panel shows the ice mixing ratio ( $\text{g kg}^{-1}$ ) and the bottom panel shows the vertical ice flux ( $\text{g kg}^{-1} \text{m s}^{-1}$ ). The small side panel shows the domain mean profiles, except for the top panel where the buoyant moist updraft mass flux (see the text for a definition) is plotted ( $\text{kg m}^{-2} \text{s}^{-1}$ ).*

with a vertical flux of ice across the inversion of  $0.11 \text{g kg}^{-1} \text{s}^{-1}$  compared to a time mean transport of ice across the inversion of  $0.011 \text{g kg}^{-1} \text{s}^{-1}$ .

The top panel of figure 5 shows the vertical velocity at a later stage during the develop-

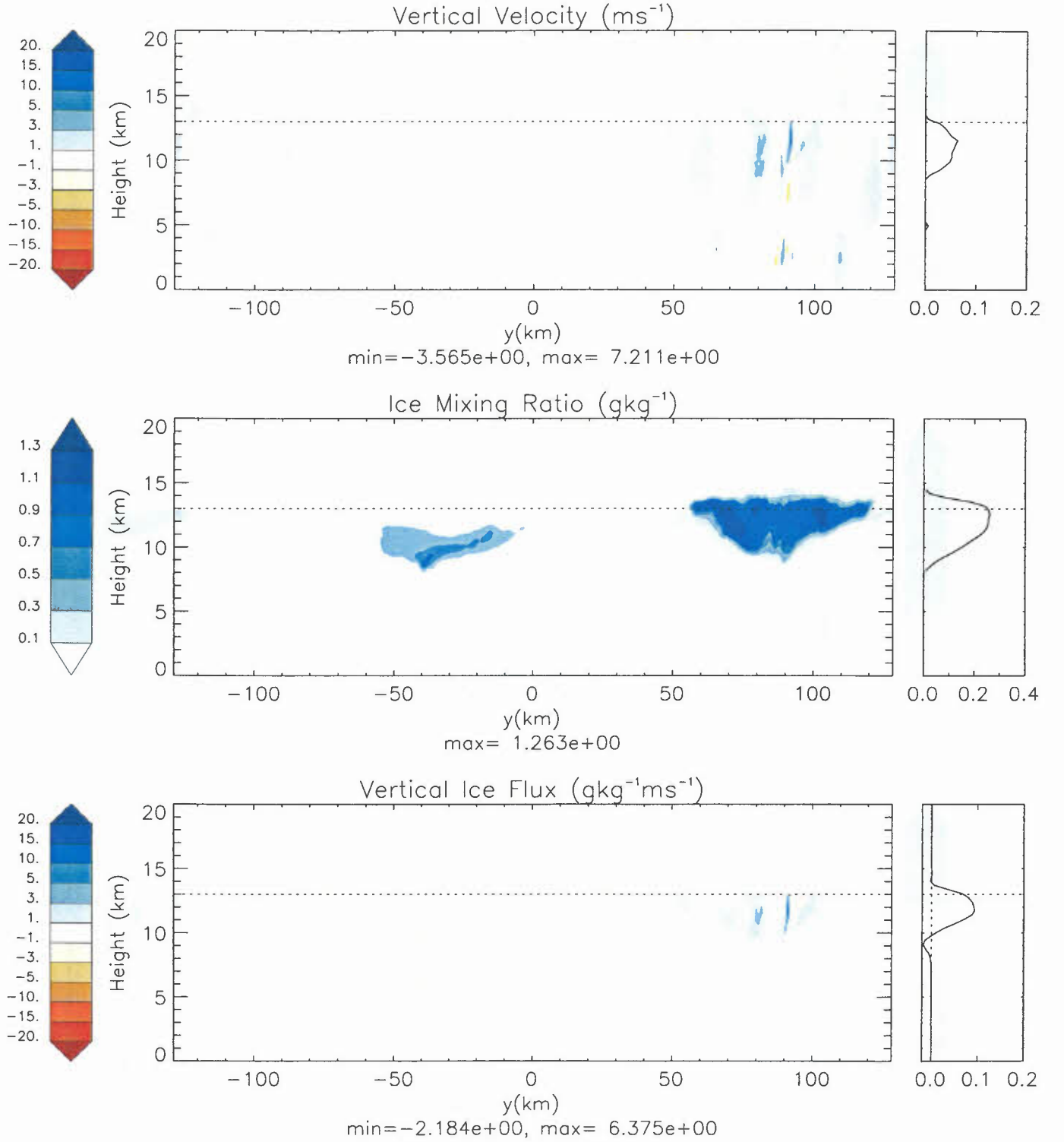


Figure 5: As for figure 4 except after 85 hours.

ment of a (different) deep convective cloud . There is still a large buoyant updraft circulation in the upper part of the troposphere, but there is no longer a single plume and there is a large amount of gravity wave activity around the convection. The ice anvil associated with the convection has a much large horizontal extent than in figure 4 and the domain mean ice is greater. The total flux of ice across the inversion is no longer dominated by the transport in a single plume, but has a significant contribution from a larger area of smaller transports associated with the gravity waves within in the ice anvil. The total flux at this time is

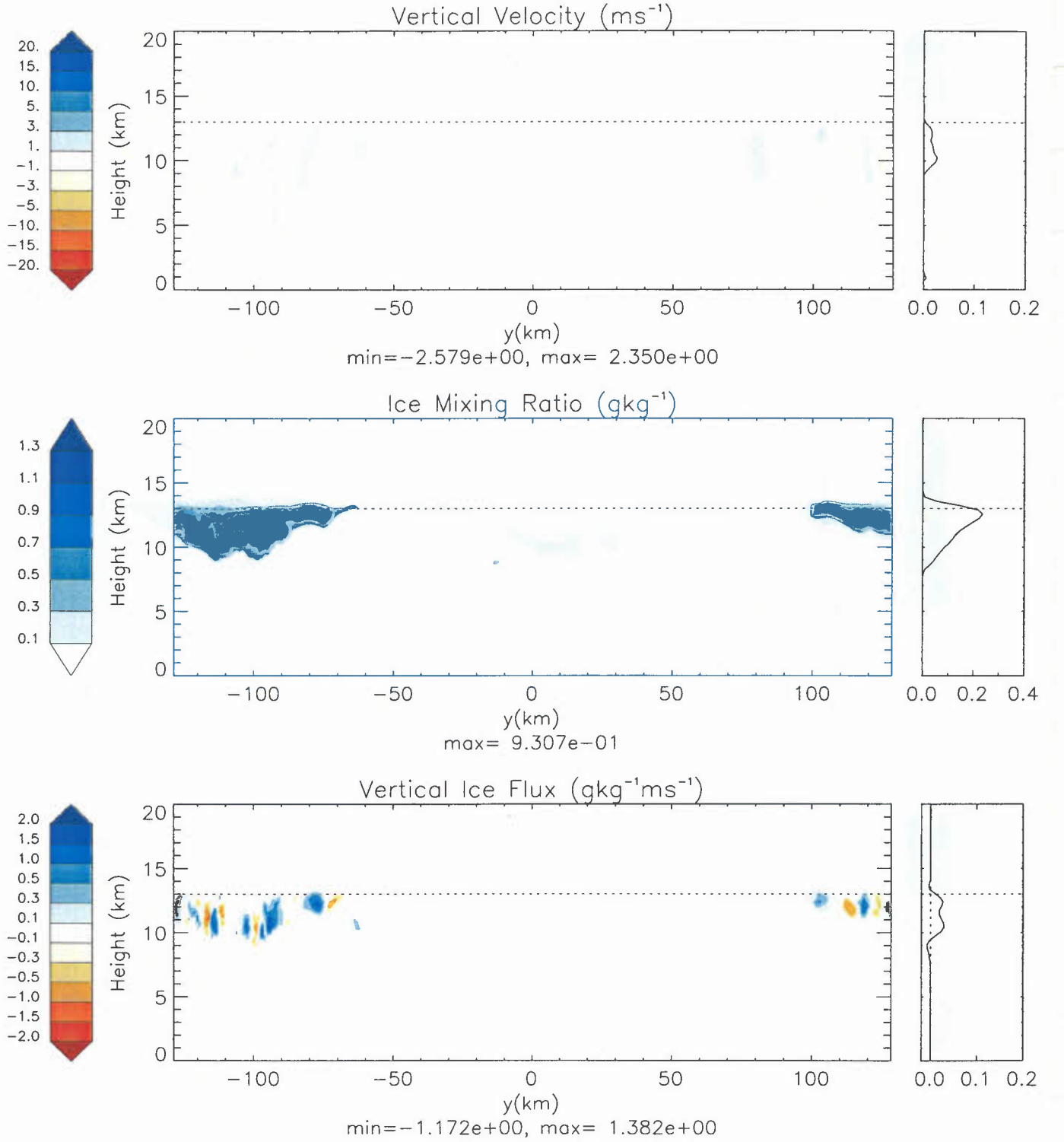


Figure 6: As for figure 4 except after 70 hours (one hour after figure 4). Note that the contour interval in the bottom panel is one-tenth of that in figures 4 and 5.

$0.066\text{gkg}^{-1}\text{s}^{-1}$ , still much larger than the time mean circulation, but smaller than at the time shown in figure 4.

Figure 6 shows the instantaneous fields one hour after those in figure 4. There is no longer any indication of the strong updraft which was present an hour earlier, and there is only a small amount of gravity wave activity. The ice anvil has a still larger horizontal extent, but with smaller ice concentrations in the clouds. The flux of ice across the tropopause is much

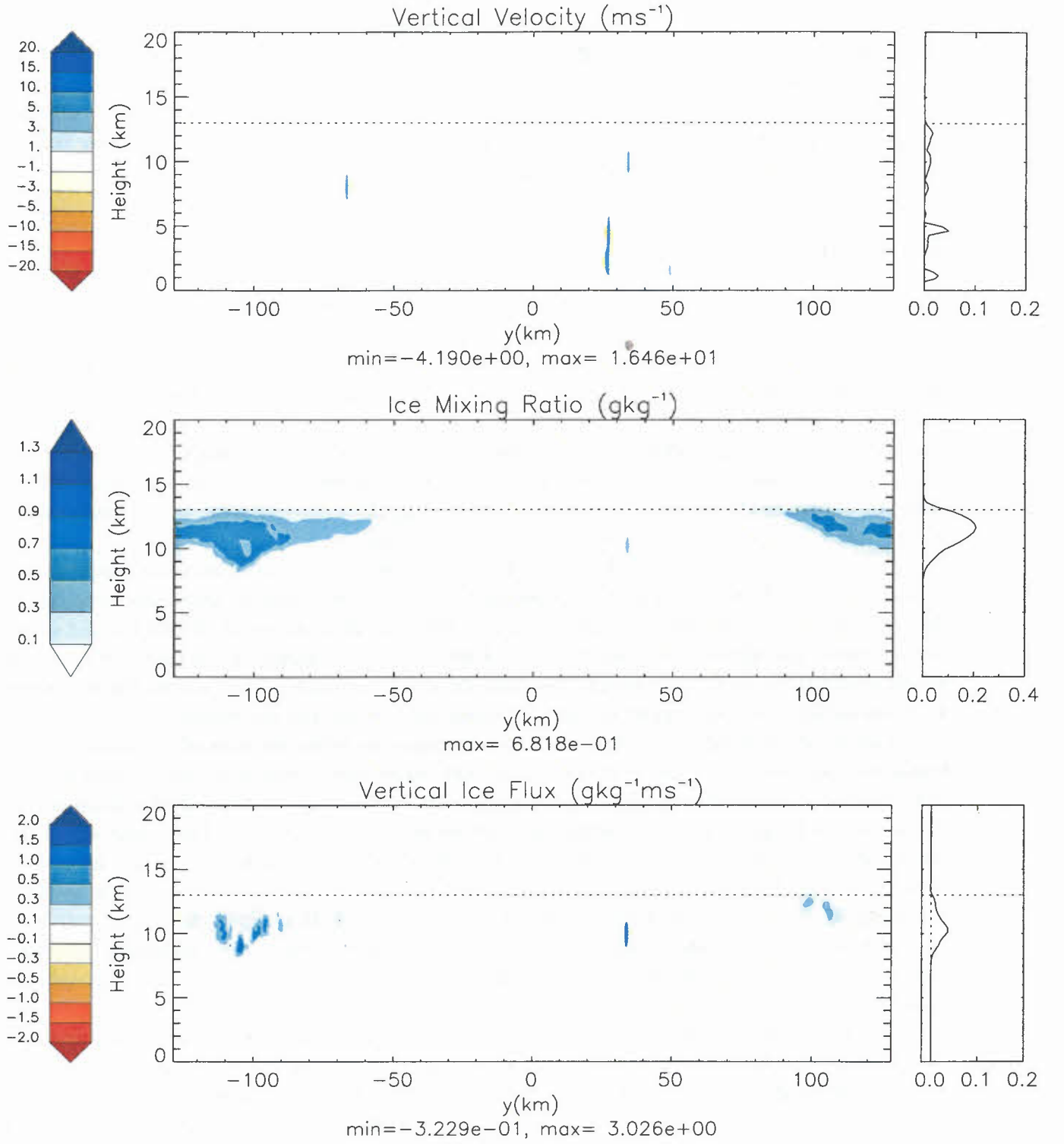


Figure 7: As for figure 4 except after 71 hours (two hours after figure 4). Note that the contour interval in the bottom panel is one-tenth of that in figures 4 and 5.

reduced with the domain mean flux now only  $0.009 \text{ g kg}^{-1} \text{ s}^{-1}$ , which is of the same order as the time mean flux.

Figure 7 shows the fields two hours after figure 4. The only remaining sign of the convection is the ice anvil which has spread further horizontally with a reduction in the ice concentrations. The domain mean ice flux is now only  $0.0017 \text{ g kg}^{-1} \text{ s}^{-1}$ , just 15% of the time mean transport.



These cross-sections indicate that most of the transport of ice across the inversion in these integrations is associated with deep convection. Most of this transport occurs within deep penetrating plumes, which are not necessarily buoyant at the inversion, in the early stages of the deep convective cloud. There is some additional transport by the vertical motions in the gravity waves associated with the mature stages of the convection, but there is little transport by turbulent mixing in the long-lived ice anvils.

## 4 Conclusions

A series of Cloud Resolving Model experiments have been performed to investigate the transport of water across a tropopause like inversion by convection.

For the experiments with the inversion at 10km and SSTs of 27°C and 29°C the inversion temperatures are above -38°C, the threshold for homogenous freezing in the microphysical scheme. The dominant source of water vapour above the inversion is by the transport of vapour and cloud liquid. However this combination of high SST and low inversion (tropopause) are not observed in the Earth's atmosphere, and because this and the different nature of the above inversion water budget in these integrations, no further analysis of the 'warm integrations' was done.

Analysis of the water-vapour budget in the 'cold integrations' with inversion temperatures lower than -38°C have shown that the dominant source of water vapour above the inversion in these conditions is from the sublimation of ice. Subsequent analysis of the ice budget above the inversion has shown that the fraction of ice which is transported across the inversion which sublimates can be very small, less than 1% of the ice transported across the inversions at 15km sublimated, with most of the ice falling back below the inversion.

Analysis of the temporal variability and instantaneous cross sections of the water vapour transport indicates that most of this ice transport across the inversion occurs in deep convection, mainly through the transport associated with overshooting plumes and mixing within the ice anvils by gravity waves during the mature stage of convection. There was very little transport of ice across the inversion in the long-lived cirrus clouds which remain after deep convection has decayed. There is very little vertical motion in these cirrus clouds in these integrations, but if interactive radiation had been included in these runs then there may have been enhanced mixing due to convective overturning in the cirrus clouds, although Danielsen (1982) suggests that such convective overturning would lead to dehydration, through enhanced sedimentation.

In view of the large part that the sublimation of ice plays as a source of water vapour above the inversion due to convection and the relatively small part that the sublimation of ice plays in the total budget of ice above the inversion it is likely that the water vapour budget and hence total water vapour above the inversion will very sensitive to both the ice microphysics and ice fall speeds. There is a substantial amount of uncertainty about the specification of both the ice-microphysics and fall speeds within the CRM (due to a substantial uncertainty about these process) and as such reliable quantitative estimates of the contribution that deep convection may play as a source of water vapour in the tropical stratosphere will be difficult to obtain from these integrations. Improvements in the understanding and representation of ice microphysics are therefore an essential step to improving our understanding of the role that the convective transport of water across the tropopause plays in the total stratospheric water budget. However, an estimate of the sensitivity of the water budget to these terms could be obtained by varying the parameters within the existing schemes.

The introduction of some representation of interactive radiation would allow Danielsen's

hypothesis to be tested, but once again the net transport of water across the tropopause by this mechanism is likely to be very sensitive to the specification of the ice-microphysics and ice fall speeds. Given that both of these potentially competing mechanisms for ice-transport are likely to be sensitive to the same parameters, any investigations of Danielsen's hypothesis and its sensitivity to the ice-microphysics should take full account of the sensitivity of the ice transport by penetrating plumes and mixing in gravity waves to these parameters, e.g. through parallel integrations without radiation.

Given the poor representation in GCMs of both the microphysical processes and the overshooting convection and mixing within the ice-anvils responsible for the transport of ice across the inversion, GCMs are unlikely to model this convective source of stratospheric water vapour well. The poor representation of this process in GCMs will make determining the role that it plays in the total stratospheric water budget difficult and may make a significant contribution to the errors in the modelling of stratospheric water vapour in GCMs.

## References

- Brewer, A. W. (1949). Evidence for a world circulation provided by the measurements of helium and water vapour distribution in the stratosphere. *Quart. J. R. Met. Soc.*, **75**, 351–363.
- Brown, A. R., Gray, M. E. B., and MacVean, M. K. (1997). Large-eddy simulation on a massively parallel computer. *Met O (APR) Turbulence and Diffusion Note No. 240*.
- Danielsen, E. F. (1982). A dehydration mechanism for the stratosphere. *Geophys. Res. Lett.*, **9**, 605–608.
- Derbyshire, S. H., Brown, A. R., and Lock, A. P. (1994). The Meteorological Office Large-Eddy Simulation Model. *Met O (APR) Turbulence and Diffusion Note No. 213*.
- Dobson, G. M. B. (1956). Origin and distribution of the polyatomic molecules in the atmosphere. *Proc. R. Soc. London*, **A236**, 187–193.
- Gray, M. E. B., Petch, J., Derbyshire, S. H., Brown, A. R., Lock, A. P., and Swann, H. A. (2001). Version 2.3 Of The Met Office Large Eddy Model: Part II. Scientific Documentation. *Met O (APR) Turbulence and Diffusion Note No. 276*.
- Jackson, D. R., Driscoll, S. J., Highwood, E. J., Harries, J. E., and Russell III, J. M. (1998). Troposphere to stratosphere transport at low latitudes as studied using HALOE observations of water vapour 1992–1997. *Quart. J. R. Met. Soc.*, **124**, 169–192.
- Kley, D., Schmeltekopf, A. L., Kelly, K., Winkler, R. H., Thompson, T. L., and McFarland, M. (1982). Transport of water through the tropical tropopause. *Geophys. Res. Lett.*, **9**, 617–620.
- Mote, P. W., Rosenlof, K. H., Holton, J. R., Harwood, R. S., and Walters, J. W. (1995). Seasonal variations of water vapour in the tropical lower stratosphere. *Geophys. Res. Lett.*, **22**, 1093–1096.
- Mote, P. W., Rosenlof, K. H., McIntyre, M. E., Carr, E. S., Kinnnersley, J. S., Pumphrey, H. C., Harwood, R. S., Holton, J. R., Russell III, J. M., Walters, J. W., and Gille, J. C. (1996). An atmospheric tape recorder: the imprint of tropical tropopause temperatures on stratospheric water vapour. *J. Geophys. Res.*, **101**, 3989–4006.